



Cite this: *Phys. Chem. Chem. Phys.*,  
2015, 17, 25342

## Branching ratios for the reactions of OH with ethanol amines used in carbon capture and the potential impact on carcinogen formation in the emission plume from a carbon capture plant†

L. Onel,<sup>\*a</sup> M. A. Blitz,<sup>ab</sup> J. Breen,<sup>a</sup> A. R. Rickard<sup>cd</sup> and P. W. Seakins<sup>\*ab</sup>

The OH initiated gas-phase chemistry of several amines that are potential candidates for use in post-combustion carbon capture (PCCC) plants have been studied by laser flash photolysis with OH monitored by laser induced fluorescence. The rate coefficients for the reaction of OH with *N*-methylethanolamine (MMEA) and *N,N*-dimethylethanolamine (DMEA) have been measured as a function of temperature ( $\sim 300$ – $500$  K):

$$k_{\text{OH+MMEA}} = (8.51 \pm 0.65) \times 10^{-11} \left( \frac{T}{298} \right)^{-(0.79 \pm 0.22)}, \quad k_{\text{OH+DMEA}} = (6.85 \pm 0.25) \times 10^{-11} \left( \frac{T}{298} \right)^{-(0.44 \pm 0.12)}.$$

The results for DMEA lie between previous values. This is the first kinetic study of the OH + MMEA reaction. At low pressures in the presence of oxygen, OH is recycled in the DMEA reaction as has been observed for other tertiary amines. Branching ratios for OH abstraction with MEA, DMEA and MMEA are dominated by abstraction from the  $\alpha\text{CH}_2$  group. Abstraction from N-H is determined to be  $0.38 \pm 0.06$  for MEA and  $0.52 \pm 0.06$  for MMEA at 298 K. The impact of these studies has been assessed by using a modified chemical box model to calculate downwind concentrations of nitramines and nitrosamine formed in the photo-oxidation of MEA. Under clear sky conditions, the simulations suggest that current safe guidelines for nitramines may be significantly exceeded with predicted MEA emission rates.

Received 13th July 2015,  
Accepted 2nd September 2015

DOI: 10.1039/c5cp04083c

[www.rsc.org/pccp](http://www.rsc.org/pccp)

### 1. Introduction

One of the most feasible options for the mitigation of carbon dioxide emissions from fossil fuel power stations is post-combustion carbon capture (PCCC) using amines.<sup>1–4</sup> Monoethanolamine (MEA) is considered as a benchmark solvent in terms of performance, and has been extensively investigated for use as a PCCC solvent although amines blends are most likely to be used in commercial applications.<sup>3,5–7</sup> A range of amines are being investigated, including other primary amines such as 2-amino-2-methylpropan-1-ol, secondary amines such as piperazine (PZ) and diethanolamine, and tertiary amines such as *N*-methyldiethanolamine (MDEA) and triethanolamine.<sup>8</sup>

Other ethanolamines such as *N*-methylethanolamine (MMEA) and *N,N*-dimethylethanolamine (DMEA) have also been studied as PCCC potential solvents, and for our studies are useful model systems to help understand issues associated with the formation of toxic degradation products in the atmosphere.<sup>9,10</sup> In addition, both MMEA and DMEA have been identified as potential products of the *in situ* degradation of MDEA during natural gas desulphurization and PCCC.<sup>8,11</sup>

Given the substantial volumes of amines needed for efficient CO<sub>2</sub> capture, large scale use of PCCC will potentially result in significant amine emissions to the atmosphere. A PCCC plant using MEA to remove  $\sim 1$  Mt CO<sub>2</sub> per year is predicted to emit 40–160 tonnes of MEA per year.<sup>12</sup> Previous studies of MEA, PZ and methylamines have shown that, once these amines are released into the atmosphere, their gas-phase processing, primarily initiated by OH radical reactions, will compete with heterogeneous uptake (lifetimes range from 15 min – 1 hour at peak OH concentrations, typically  $5 \times 10^6$  molecule cm<sup>−3</sup>).<sup>13–18</sup> The atmospheric removal of amines by reaction with Cl atoms in gas-phase has been found to be a minor sink for amines (lifetime of  $\sim 20$  days for typical peak Cl concentrations, around  $2 \times 10^3$  atom cm<sup>−3</sup>).<sup>19,20</sup> A major concern with PCCC is the impact of carcinogenic nitrosamines (R<sub>2</sub>N-NO) and nitramines

<sup>a</sup> School of Chemistry, University of Leeds, Leeds, LS2 9JT, UK. E-mail: chmlo@leeds.ac.uk

<sup>b</sup> National Centre for Atmospheric Science (NCAS), University of Leeds, Leeds, LS2 9JT, UK

<sup>c</sup> Wolfson Atmospheric Chemistry Laboratories, Department of Chemistry, University of York, York, YO10 5DD, UK

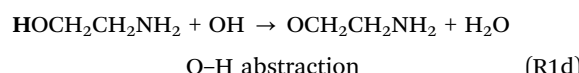
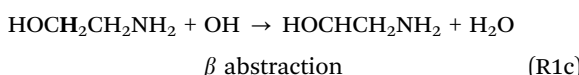
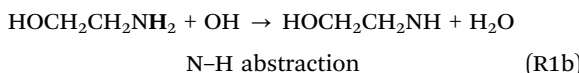
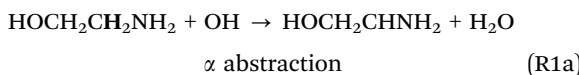
<sup>d</sup> National Centre for Atmospheric Science (NCAS), University of York, York, YO10 5DD, UK

† Electronic supplementary information (ESI) available: Details on OH + DMEA reaction in the absence/presence of O<sub>2</sub>, OH/OD + d<sub>4</sub>-DMEA reaction with O<sub>2</sub>, OH + MEA/MMEA/MeOEA reactions in the presence of O<sub>2</sub>/NO, SAR calculations, MESMER calculations and atmospheric modelling. See DOI: 10.1039/c5cp04083c



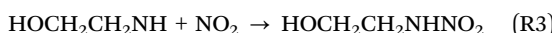
( $\text{R}_2\text{N}-\text{NO}_2$ ), formed in the gas-phase processing of amines, on human health.<sup>19,21–24</sup> The yield of these toxic products depends on the fraction of amine processed in the gas-phase (hence on the overall rate coefficient for the OH + amine reaction), and on the branching ratios in the initial OH abstraction reaction.

MEA has four potential sites for OH abstraction:



Previous determinations of the branching ratios in reaction (R1) used analysis of concentration profiles of secondary-generated products obtained by chamber experiments<sup>23,25</sup> and theoretical calculations.<sup>26</sup> Experiments carried out in the European Photoreactor (EUPHORE) suggested that >80% of the initial OH abstraction occurs through reaction (R1a). In contrast, the theoretical work of Xie *et al.* found that  $\alpha\text{C-H}:\beta\text{C-H} = 0.39:0.43$ ,<sup>26</sup> while calculations using the structure-activity relationships (SARs) predict that  $\alpha\text{C-H}:\text{N-H} = 0.45:0.47$  (Table S2, ESI<sup>†</sup>).<sup>19,27,28</sup>

The N-centred radical generated by reaction (R1b) reacts with NO and  $\text{NO}_2$  to form 2-nitrosoaminoethanol,  $\text{HOCH}_2\text{CH}_2\text{NHNO}$  and 2-nitroaminoethanol,  $\text{HOCH}_2\text{CH}_2\text{NHNO}_2$  respectively (reactions (R2) and (R3)). Reactions (R2) and (R3) are potentially in competition with reaction (R4) forming 2-iminoethanol,  $\text{HOCH}_2\text{CHNH}$ ; little is known about (R4), but it is predicted to be slow ( $\sim 1 \times 10^{-19} \text{ cm}^3 \text{ molecule}^{-1} \text{ s}^{-1}$ ).<sup>23,29</sup>



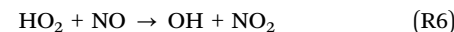
$\text{HOCH}_2\text{CH}_2\text{NHNO}$  was not detected in the EUPHORE studies.<sup>23,25</sup> The theoretical calculations of Tang *et al.* conclude that primary nitrosamines,  $\text{RCH}_2\text{NH}-\text{NO}$ , are not stable and rapidly form imines by isomerization to  $\text{RCHNHNOH}$  followed by reaction with  $\text{O}_2$ .<sup>30</sup> However, based on the theoretical study of da Silva,  $\text{RNH}-\text{NO}$  are significant products in  $\text{RNH} + \text{NO}$  reactions.<sup>31</sup>

The branching ratio for the abstraction at the N-H site,  $r_{1b}$ , was reported to be <0.10 by Nielsen *et al.*,<sup>25</sup> 0.15 by Karl *et al.*<sup>23</sup> and 0.17 by Xie *et al.*<sup>26</sup> The SAR calculations lead to  $r_{1b} = 0.47$ .<sup>19,27,28</sup> Given the discrepancies between the reported branching ratios in reaction (R1), there is a clear need for the direct experimental determination of  $r_{1a} - r_{1d}$ .

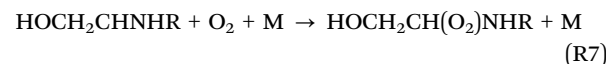
The overall rate coefficient  $k_{\text{OH+MMEA}}$  and the branching ratios in the reactions of OH with MMEA ( $\text{HOCH}_2\text{CH}_2\text{NH}(\text{CH}_3)$ ) and DMEA ( $\text{HOCH}_2\text{CH}_2\text{N}(\text{CH}_3)_2$ ) have not previously been studied.

Here we report on the determination of the rate coefficients of OH + MMEA and DMEA reactions and their temperature dependence using laser flash photolysis (LFP) for OH generation and laser induced fluorescence (LIF) for time-resolved OH monitoring. We find OH regeneration in the OH + DMEA reaction in the presence of oxygen. The OH/OD signals obtained by 248 nm photolysis of  $(\text{CH}_3)_2\text{N}(\text{CD}_2)_2\text{OH}$  ( $d_4\text{-DMEA}$ ) in the presence of  $\text{O}_2$  are then used to determine the dominant H-abstraction site for DMEA.

On the millisecond scale of the OH + MEA/ $\text{O}_2/\text{NO}$  and OH + MMEA/ $\text{O}_2/\text{NO}$  LFP/LIF experiments,  $\text{HO}_2$  is generated through reaction (R5) and reacts further with NO (reaction (R6)) to give back OH.



The  $\text{HO}_2$  yield and the branching ratios in the initial OH reaction are determined using the method developed previously for OH reactions with amines such as dimethylamine (DMA) and ethylamine (EA).<sup>32</sup> Calculations using the MESMER (Master Equation Solver for Multi-Energy Well Reactions) package<sup>33</sup> show that, at the relatively low pressures used in our experiments, the  $\text{O}_2$  addition producing a stabilised peroxy species (reaction (R7)) does not compete with reaction (R5) to affect our results. However, the  $\text{O}_2$  addition is in competition with  $\text{O}_2$  abstraction at atmospheric pressure.



The impact of this work on the downwind formation of nitrosamines and nitramines following emission of MEA from a typical PCCC plant is assessed using an atmospheric chemistry box model. MEA and  $\text{NO}_x$  emissions are based on the PCCC pilot plant located at Mongstad, on the west coast of Norway.<sup>24,34</sup> The model also incorporates typical gas-phase chemistry of background compounds and MEA, heterogeneous uptake and reactions, and plume dispersion described by a time dependent Gaussian equation.

## 2. Experimental

This work has been carried out in a slow-flow pulsed LFP-LIF system that has been described in several previous publications.<sup>13,16,32</sup> The flows of the OH/OD precursor, amine (MEA and DMEA: Sigma-Aldrich,  $\geq 99.5\%$ , MMEA and 2-methoxyethylamine (MeOEA): Alfa Aesar, 99%),  $\text{O}_2$  (if used, BOC 99.999%), nitrogen monoxide (if used, BOC > 99.9%) and bath gas ( $\text{N}_2$ , BOC oxygen free) were regulated through calibrated mass flow controllers, mixed in a manifold and introduced into a stainless steel reactor. The OH precursor was tertiary butylhydroperoxide (Sigma-Aldrich, 70% in water) and the OD precursor was deuterated acetone (acetone- $d_6$ ) in the presence of  $\text{O}_2$ <sup>35</sup> or  $(\text{CH}_3)_3\text{COOD}/\text{N}_2 + \text{D}_2\text{O}$ .<sup>32</sup> The total pressure in the cell was controlled *via* a needle valve on the exhaust line and measured using a capacitance manometer. Temperatures were measured close to the observation region using a K-type thermocouple.



DMEA was prepared as a diluted mixture in nitrogen in a glass bulb. Gaseous mixtures of MEA and MMEA could not be prepared because of the low vapour pressures of these amines at 298 K.<sup>36</sup> Therefore, MEA and MMEA were introduced into the reactor from a glass bubbler by flowing N<sub>2</sub> gas over liquid amine samples. The concentrations of MEA and MMEA were determined using the technique developed previously using *in situ* absorption measurements at 185 nm.<sup>16,18</sup> Absorptions were converted into concentrations using the absorption cross sections of amines,  $\sigma_{185\text{ nm, MEA}} = (8.53 \pm 0.24) \times 10^{-18} \text{ cm}^2 \text{ molecule}^{-1}$ ,<sup>16</sup> and  $\sigma_{185\text{ nm, MMEA}} = (9.71 \pm 0.37) \times 10^{-18} \text{ cm}^2 \text{ molecule}^{-1}$  (this work).

Radicals were generated by excimer laser flash photolysis at 248 nm (Lambda Physik 210, typically 5–15 mJ cm<sup>−2</sup>, 5 Hz repetition rate). OH radicals were probed by off-resonance laser induced fluorescence at an excitation wavelength of ~282 nm generated from a YAG pumped dye laser (Powerlite Precision II 8010, Sirah PRSC-DA-24, operating with Rhodamine 6G dye) introduced perpendicularly to the photolysis laser. OH fluorescence centred at 308 nm was observed with a photomultiplier tube (Thorn EMI model 9813 QKB) through an interference filter (Andover, 308 ± 10 nm). The time delay between the photolysis and the probe laser was varied using an in-house LabView program to build up an entire time-dependent OH profile. Depending on signal to noise ratios, 6–20 laser shots were averaged for each time point.

## 2.1. OH + amine reactions in the absence of NO

The reactions were carried out under pseudo-first-order conditions using amine concentrations in large excess over the initial OH concentration (~1000:1). Under these conditions, in the absence of NO, the fluorescence intensity,  $I_f$ , which is proportional to [OH], decayed according to the single exponential eqn (E1) (see the inset of Fig. 1 and Fig. S1 as examples, ESI<sup>†</sup>).

$$I_f(t) = I_f(0) \exp(-k_{\text{OH}'} t) \quad (\text{E1})$$

where  $k_{\text{OH}'} = k_{\text{OH}}[\text{amine}] + k_{\text{loss}}$ . Here  $k_{\text{OH}}$  is the bimolecular rate coefficient for the reaction of OH with amine and  $k_{\text{loss}}$  is the pseudo-first-order rate coefficient for OH loss by diffusion and reaction with OH precursor. Fig. 1 shows an example of bimolecular plot for the OH + MMEA reaction. The error in the bimolecular rate coefficient is a combination in quadrature of statistical error at the 2 $\sigma$  level and an estimated 10% systematic error.

For the reaction OH + DMEA in the presence of O<sub>2</sub>, the experiments were performed using sufficiently high O<sub>2</sub> concentration (~10<sup>16</sup> molecule cm<sup>−3</sup>) to obtain single exponential OH decays. Examples of bimolecular plots for the DMEA + OH reaction in the absence/presence of O<sub>2</sub> are shown in Fig. S1 (ESI<sup>†</sup>).

## 2.2. OH + MEA/MMEA and OD + deuterated MEA/MMEA reactions in the presence of O<sub>2</sub>/NO

Pseudo-first-order conditions were ensured by having amine (0.5–6.0 × 10<sup>14</sup> molecule cm<sup>−3</sup>), O<sub>2</sub> and NO concentrations in great excess over the initial radical concentration (0.5–2.0 × 10<sup>11</sup> molecule cm<sup>−3</sup>). The O<sub>2</sub> concentration was higher by a

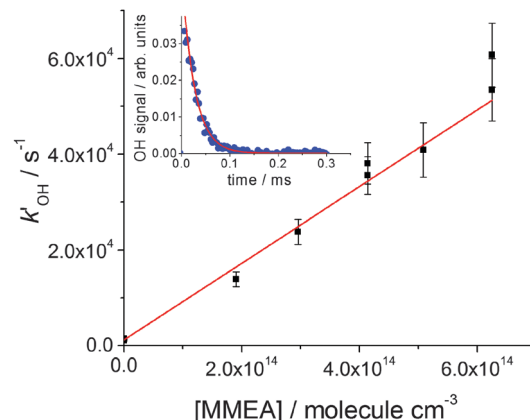


Fig. 1 Bimolecular plot for MMEA,  $(8.01 \pm 0.92) \times 10^{-11} \text{ cm}^3 \text{ molecule}^{-1} \text{ s}^{-1}$ , at 298 K and a total pressure of 17 Torr of N<sub>2</sub>. The error bars are at 2 $\sigma$  level. A typical OH fluorescence decay trace and fit to eqn (E1) is shown in the inset.

factor of ~100 than the NO concentration and typically [NO] = 0.1–1.0 × 10<sup>15</sup> molecule cm<sup>−3</sup>. Biexponential decays of OH were generated under these conditions due to reaction (R6) regenerating OH and were analysed as described previously.<sup>32</sup>

In the reactions of OD with DOCH<sub>2</sub>CH<sub>2</sub>ND<sub>2</sub> (*d*<sub>3</sub>-MEA) and DOCH<sub>2</sub>CH<sub>2</sub>ND(CH<sub>3</sub>) (*d*<sub>2</sub>-MMEA) (CH<sub>3</sub>)<sub>3</sub>COOD was used as OD precursor. The deuteration of amine and radical precursor were achieved by H/D exchange in the delivery tubing of the cell using D<sub>2</sub>O (99.9 atom% D), as described elsewhere.<sup>32</sup>

## 2.3. Synthesis of [1,1,2,2-<sup>2</sup>H<sub>4</sub>]-2-dimethylaminoethanol (*d*<sub>4</sub>-DMEA)

Ethyl 2-(dimethylamino)-2-oxoacetate (5.00 g, 34.4 mmol) was added slowly over 20 min to a stirred solution of LiAlD<sub>4</sub> (3.47 g, 82.6 mmol) in dry THF (200 mL) at 0 °C. The mixture was heated under reflux for 6 h and the reaction cooled to 0 °C. The reaction was quenched by the drop-wise addition of saturated Na<sub>2</sub>SO<sub>4</sub> solution until effervescence ceased and a white solid formed. After stirring for 30 min, the precipitate was collected by filtration and extracted into tetrahydrofuran (600 mL) by Soxhlet extraction for 18 hours to give a pale yellow solution. The solvent was removed *in vacuo* to give a yellow oil, which was purified by distillation (131–134 °C), to give *d*<sub>4</sub>-DMEA (1.98 g, 62%) as a colourless oil; <sup>1</sup>H NMR (500 MHz, CDCl<sub>3</sub>): δ 2.04 (6H, s, CH<sub>3</sub>); <sup>13</sup>C NMR (125 MHz, CDCl<sub>3</sub>): δ 45.2 (CH<sub>3</sub>), 57.9 (<sup>1</sup>J<sub>CD</sub> 21.7, CD<sub>2</sub>N), 60.0 (<sup>1</sup>J<sub>CD</sub> 20.2, CD<sub>2</sub>OH); *m/z* (EI<sup>†</sup>) 93.1.

## 3. Results and discussion

### 3.1. Kinetics of OH + MMEA and DMEA

The averages of the measured room temperature rate coefficients,  $k_{\text{OH+MMEA}} = (8.26 \pm 0.82) \times 10^{-11} \text{ cm}^3 \text{ molecule}^{-1} \text{ s}^{-1}$  and  $k_{\text{OH+DMEA}} = (7.29 \pm 0.72) \times 10^{-11} \text{ cm}^3 \text{ molecule}^{-1} \text{ s}^{-1}$ , are similar to  $k_{\text{OH+MEA}} = (7.61 \pm 0.76) \times 10^{-11} \text{ cm}^3 \text{ molecule}^{-1} \text{ s}^{-1}$ .<sup>16</sup> The results are in good agreement with  $k_{\text{OH}}/10^{-11} \text{ cm}^3 \text{ molecule}^{-1} \text{ s}^{-1}$  obtained using the SARS:<sup>19,27,28</sup> 8.45 for MMEA and 6.95 for DMEA (see Table S2, ESI<sup>†</sup>). This is the first determination of  $k_{\text{OH+MMEA}}$ . The room temperature value for the OH + DMEA reaction is in



between the measurement of Harris and Pitts,  $(4.7 \pm 1.2) \times 10^{-11} \text{ cm}^3 \text{ molecule}^{-1} \text{ s}^{-1}$ ,<sup>37</sup> and the measurement of Anderson and Stephens,  $(10.3 \pm 2.0) \times 10^{-11} \text{ cm}^3 \text{ molecule}^{-1} \text{ s}^{-1}$ .<sup>38</sup> Both previous studies used the photolysis of water in the VUV ( $\lambda \geq 105 \text{ nm}$ <sup>37</sup> and  $\lambda > 160 \text{ nm}$ <sup>38</sup>) to generate OH, which was probed by resonance fluorescence using a microwave discharge lamp. The measurement of Anderson and Stephens almost overlaps with our measurement. The finding of OH recycling in the OH + DMEA/O<sub>2</sub> system described in the next section offers a possible explanation for the lower rate coefficient found by Harris and Pitts if small amounts of oxygen were present in these experiments.

Fig. 2 shows the temperature dependence of  $k_{\text{OH+MMEA}}$  and  $k_{\text{OH+DMEA}}$ . The negative temperature dependence observed for MMEA is similar to the temperature dependence found for MEA.<sup>16</sup> The rate coefficient for OH + DMEA reaction decreases more slowly with temperature and at 500 K is about 85% relative to the value at 298 K. The result is consistent with the only other temperature dependent study for OH + DMEA reaction, which reports no evident temperature dependence over the range 234–364 K.<sup>38</sup>

In addition, the reaction between DMEA and OD was studied. As it can be observed in Fig. 2, the rate coefficients for OH + DMEA and OD + DMEA are similar, suggesting a minimal isotope effect. This result is in agreement with our previous finding that the rate coefficients for the reactions of methylamines with OH and OD are similar.<sup>13</sup>

### 3.2. Kinetics of OH + MEA, MMEA and DMEA reactions in the presence of oxygen

Fig. S1 (ESI†) shows examples of bimolecular plots for OH + DMEA reaction obtained using N<sub>2</sub> (100%) and O<sub>2</sub> (10%) + N<sub>2</sub> (90%), respectively. It can be clearly seen that the bimolecular rate coefficient in the presence of excess O<sub>2</sub>,  $k_{\text{O}_2}$ , is lower than

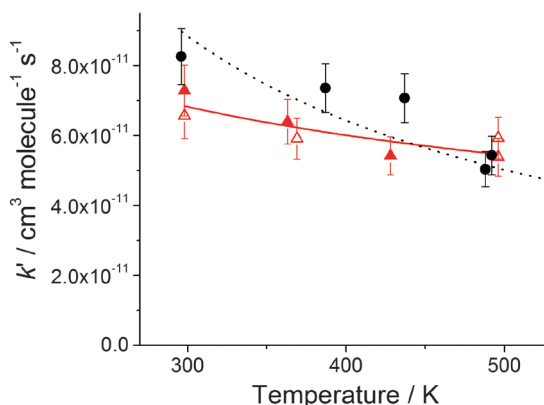
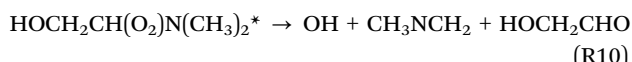
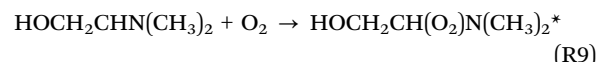
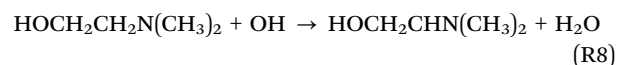


Fig. 2 Temperature dependence of the rate coefficient for the OH + MMEA reaction (black circles) and the OH/OD + DMEA reaction (red solid/open triangles). The OH kinetic data can be represented by the following parameterizations ( $\text{cm}^3 \text{ molecule}^{-1} \text{ s}^{-1}$ ):  $k_{\text{OH+MMEA}} = (8.51 \pm 0.65) \times 10^{-11} \left(\frac{T}{298}\right)^{-(0.79 \pm 0.22)}$  (black dot line),  $k_{\text{OH+DMEA}} = (6.85 \pm 0.25) \times 10^{-11} \left(\frac{T}{298}\right)^{-(0.44 \pm 0.12)}$  (red line).

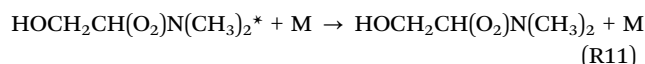
the bimolecular rate coefficient in the absence of O<sub>2</sub>,  $k_{\text{N}_2}$ , which is indicative of rapid OH regeneration. The OH yield,  $\Phi_{\text{OH}}$ , can be calculated from  $k_{\text{N}_2}$  and  $k_{\text{O}_2}$  (eqn (E2)), as shown in our previous work.<sup>13</sup>

$$\Phi_{\text{OH}} = 1 - \frac{k_{\text{O}_2}}{k_{\text{N}_2}} \quad (\text{E2})$$

Our observation of similar OH recycling for TMA (trimethylamine) + OH/O<sub>2</sub><sup>13</sup> suggests that in the case of DMEA + OH/O<sub>2</sub> the hydrogen abstraction occurs predominantly from a position next to the amine group of DMEA. Unlike TMA, not all the  $\alpha$ -hydrogens are equivalent, however, the experiments using *d*<sub>4</sub>-DMEA/O<sub>2</sub> described in ESI† show that the abstraction from the CH<sub>2</sub> group next to the amine group largely dominates over the abstraction from CH<sub>3</sub> groups. The OH recycling is the result of the reaction of O<sub>2</sub> with HOCH<sub>2</sub>CHN(CH<sub>3</sub>)<sub>2</sub> radical (reaction (R9) followed by reaction (R10)) generated by the initial abstraction (reaction (R8)).



DMEA photolysis at 248 nm in the presence of O<sub>2</sub> generates the same radical as reaction (R8), HOCH<sub>2</sub>CHN(CH<sub>3</sub>)<sub>2</sub>, which explains the fast generation of OH observed in the absence of an OH precursor. By analogy with the recycling mechanistic scheme proposed for TMA/O<sub>2</sub>,<sup>13</sup> we speculate that the by-products of OH regeneration route are *N*-methylimine, CH<sub>3</sub>NCH<sub>2</sub>, and glycolaldehyde, HOCH<sub>2</sub>CHO. The decomposition of the activated peroxy species, HOCH<sub>2</sub>CH(O<sub>2</sub>)N(CH<sub>3</sub>)<sub>2</sub><sup>\*</sup> (reaction (R10)) is in competition with collisional stabilization (reaction (R11)).



Therefore, the OH yield will decrease with increasing pressure, which indeed was confirmed by experiments performed at different pressures at temperatures of 298 and 363 K (Fig. 3). The reciprocal of the OH yield is proportional to the total gas concentration, [M]:

$$\frac{1}{\Phi_{\text{OH}}} = 1 + \frac{k_{\text{stab}}}{k_{\text{regen}}} [\text{M}] \quad (\text{E3})$$

Fig. 3 shows the Stern–Volmer plots,  $1/\Phi_{\text{OH}}$  vs. [M], for the DMEA + OH/O<sub>2</sub> system at 298 and 363 K. As expected, the Stern–Volmer gradient decreases with temperature showing that the activated peroxy radical, HOCH<sub>2</sub>CH(O<sub>2</sub>)N(CH<sub>3</sub>)<sub>2</sub><sup>\*</sup>, is generated with more energy at higher temperatures and hence dissociates in a greater fraction to eliminate OH.<sup>39</sup> The Stern–Volmer plot at 298 K is similar to that obtained for OH + *d*<sub>4</sub>-DMEA/O<sub>2</sub> at room temperature (Fig. S2, ESI†).

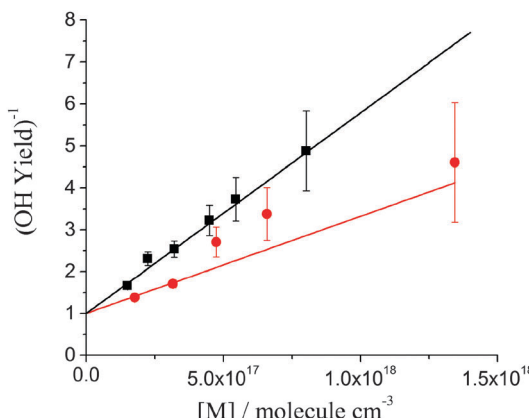


Fig. 3 Stern–Volmer plots for OH yield from DMEA + OH/O<sub>2</sub> system at 298 K, black squares and line and 363 K, red circles and line. The fits are constrained through unity intercept.

Table 1 shows the Stern–Volmer parameters and the calculated OH yields for DMEA at atmospheric pressure and 298 and 363 K. The results obtained for TMA at room temperature are also included for comparison.<sup>13</sup> At both temperatures OH regeneration by DMEA/O<sub>2</sub> is minor at atmospheric pressure. At 298 K and 1 atm  $\Phi_{\text{OH}(\text{DMEA})}$  is about two times lower than  $\Phi_{\text{OH}(\text{TMA})}$ .<sup>13</sup> The more efficient quenching of the OH + DMEA/O<sub>2</sub> is to be expected given the larger size of the system.

The observation of OH regeneration in the OH + DMEA/O<sub>2</sub> reaction, similar to that for the OH + TMA/O<sub>2</sub> reaction,<sup>13</sup> suggests that the direct OH recycling is a common feature of tertiary amines. No OH regeneration was observed in the OH + MEA/MMEA experiments with O<sub>2</sub> over the temperature range 298–500 K. In addition, no OH signal was obtained following MEA and MMEA photolysis in the presence of oxygen. This result is in line with the lack of direct OH recycling in the case of other amines containing N–H bond(s), such as methylamine, DMA and PZ.<sup>13,18</sup>

### 3.3. OH + MEA/MMEA reactions in the presence of O<sub>2</sub>/NO

The observed generation of HO<sub>2</sub> in the OH + MEA/MMEA reactions with O<sub>2</sub> may occur through OH abstraction at either the  $\alpha$  or  $\beta$  position, followed by abstraction at the N–H and O–H sites, respectively, by O<sub>2</sub>.<sup>23,32,40</sup> Therefore, the HO<sub>2</sub> yield for MEA,  $\Phi_{\text{HO}_2(\text{MEA})}$ , is equal to the sum of the branching ratios for reactions (R1a) and (R1c),  $r_{1a} + r_{1c}$ . Experiments using the OH + 2-methoxyethylamine (MeOEA)/O<sub>2</sub>/NO system give a similar fraction of HO<sub>2</sub> generation. In MeOEA, abstraction  $\beta$  to the N atom cannot lead to HO<sub>2</sub> production, suggesting that  $r_{1a} + r_{1c} \approx r_{1a}$  (ESI†), in agreement with previous experimental studies reporting that the  $\alpha$  position is the dominant abstraction site in the OH + MEA reaction.<sup>23,25</sup> Therefore,  $\Phi_{\text{HO}_2(\text{MEA})} = r_{1a}$ . The result is in disagreement with the theoretical calculations of Xie *et al.*, which found that both C–H abstractions are significant for MEA.<sup>26</sup>

Our result for MEA and the finding that the abstraction from DMEA by OH occurs predominantly from the  $\alpha$  methylene group (*vide supra*) suggest that the abstraction from the  $\alpha$  CH<sub>2</sub>

Table 1 Stern–Volmer parameters and the atmospheric pressure OH yields from the OH + DMEA/O<sub>2</sub> system at 298 and 363 K and the OH + TMA/O<sub>2</sub> system at 298 K<sup>13</sup>

T (K)	Unconstrained intercept						Intercept constrained to unity					
	Intercept <sup>a</sup>		Gradient <sup>a</sup> /cm <sup>3</sup> molecule <sup>-1</sup> /10 <sup>-18</sup>		OH yield at 760 Torr <sup>a</sup> /%		Intercept <sup>a</sup>		Gradient <sup>a</sup> /cm <sup>3</sup> molecule <sup>-1</sup> /10 <sup>-18</sup>		OH yield at 760 Torr <sup>a</sup> /%	
	DMEA	TMA	DMEA	TMA	DMEA	TMA	DMEA	TMA	DMEA	TMA	DMEA	TMA
<b>Unconstrained intercept</b>												
298	0.88 ± 0.13	0.79 ± 0.02	5.31 ± 0.66	2.33 ± 0.11	0.77 ± 0.09	1.7 ± 0.1	4.79 ± 0.26	1.99 ± 0.07	0.84 ± 0.04	2.0 ± 0.1		
<b>Intercept constrained to unity</b>												
363	0.86 ± 0.12	2.91 ± 0.48			1.69 ± 0.27		2.32 ± 0.17		2.11 ± 0.15			

<sup>a</sup> Obtained by weighting the linear fit by the error bars,  $2\sigma$ , of reciprocal of OH yield,  $1/\Phi_{\text{OH}} = 1/\left(1 - \frac{k_{\text{O}_2}}{k_{\text{N}_2}}\right)$ . Here  $\sigma$  are the standard errors calculated by the propagation of error equation using the statistical errors of  $k_{\text{O}_2}$  and  $k_{\text{N}_2}$ .

**Table 2** Yields of HO<sub>2</sub>/DO<sub>2</sub> and branching ratio for abstraction at  $\alpha$ C–H site for OH + MEA/MMEA and OD + *d*<sub>3</sub>-MEA/*d*<sub>2</sub>-MMEA reactions at 298 K

<i>p</i> (Torr)	$\Phi_{\text{HO}_2} = r_{\alpha\text{C}-\text{H}}^a$		$\Phi_{\text{DO}_2} = r_{\alpha\text{C}-\text{H}}^a$	
	MEA	MMEA	<i>d</i> <sub>3</sub> -MEA	<i>d</i> <sub>2</sub> -MMEA
15	—	—	0.71 ± 0.05 <sup>b</sup>	0.57 ± 0.09 <sup>b</sup>
20	0.64 ± 0.04 <sup>b</sup>	0.48 ± 0.03 <sup>b</sup>	—	—
30	—	—	0.75 ± 0.07 <sup>b</sup>	0.54 ± 0.06 <sup>b</sup>
40	—	0.45 ± 0.06 <sup>b</sup>	—	—
60	0.61 ± 0.06 <sup>b</sup>	0.51 ± 0.04 <sup>b</sup>	—	—
150	0.62 ± 0.07 <sup>b</sup>	—	—	—

<sup>a</sup> HO<sub>2</sub>/DO<sub>2</sub> yields was determined as described previously<sup>32</sup> and additionally presented in ESI. For MEA  $r_{\alpha\text{C}-\text{H}} = r_{1\text{a}}$ . <sup>b</sup> Combination in quadrature of statistical errors at the 2 $\sigma$  level and an estimated 5% systematic error.

group dominates in the OH + MMEA reaction as well, hence  $\Phi_{\text{HO}_2(\text{MMEA})} \cong r_{\alpha(\text{CH}_2)}$ .

The branching ratios, the HO<sub>2</sub> yield for OH + MEA/MMEA and the DO<sub>2</sub> yield for OD + *d*<sub>3</sub>-MEA/*d*<sub>2</sub>-MMEA were assigned by the method developed in previous work.<sup>32</sup> Table 2 shows the HO<sub>2</sub>/DO<sub>2</sub> yields at room temperature and several total pressures. The values in Table 2 represent the means of a series of measurements where either [NO] or [O<sub>2</sub>] was varied (typically by one order of magnitude).

The slightly higher value of  $r_{\alpha\text{C}-\text{H}}$  for *d*<sub>3</sub>-MEA and *d*<sub>2</sub>-MMEA compared to  $r_{\alpha\text{C}-\text{H}}$  for MEA and MMEA suggests that the NH<sub>2</sub> deuteration results in less abstraction from the amine group due to a small kinetic isotope effect (KIE) and is in agreement with the results for undeuterated and deuterated DMA and EA.<sup>32</sup>

Our result,  $r_{1\text{a}} = 0.62 \pm 0.06$  for MEA, is in between of the value obtained by the EUPHORE studies of Karl *et al.*,  $r_{1\text{a}} = 0.80$ <sup>23</sup> and the value predicted using the SARs (Table S2, ESI<sup>†</sup>),  $r_{1\text{a}} = 0.45$ . Our work used a direct method for determination of branching ratios, while EUPHORE studies calculated the branching ratios by modelling the observed time profiles of end-products. The maximum branching ratio for N–H abstraction is  $r_{\text{N}-\text{H}} = 1 - r_{\alpha\text{C}-\text{H}}$  and represents an upper limit for the carcinogenic compound production. For MMEA  $r_{\text{N}-\text{H}} = 0.52 \pm 0.06$ , which is 30% lower than the value obtained using the SARs,  $r_{\text{N}-\text{H}(\text{MMEA})} = 0.74$ , and is higher than the values found for the carbon capture amines MEA and PZ,  $r_{\text{N}-\text{H}(\text{MEA})} = 0.38 \pm 0.06$  and  $r_{\text{N}-\text{H}(\text{PZ})} = 0.09 \pm 0.06$ .<sup>18</sup> The result suggests that the PCCC emission of MMEA has a higher potential to form toxic compounds than the emission of MEA and PZ, although all secondary amines are of particular concern.

### 3.4. MESMER calculations for the pressure dependence of the HOCH<sub>2</sub>CHNH<sub>2</sub> + O<sub>2</sub> reaction

Reaction (R1a) generates an  $\alpha$  carbon-centred radical, HOCH<sub>2</sub>CHNH<sub>2</sub>, known to react with O<sub>2</sub> in the atmosphere. At low pressures the oxygen reaction occurs predominantly through O<sub>2</sub> abstraction, producing HO<sub>2</sub> and 2-iminoethanol (reaction (R5)), while at high pressures O<sub>2</sub> addition, forming a collisionally stabilised peroxy species (reaction (R7)), dominates. EUPHORE chamber studies proposed that at atmospheric pressure the HOCH<sub>2</sub>CHNH<sub>2</sub> + O<sub>2</sub> reaction proceeds 100% through reaction (R7).<sup>23,25</sup> In contrast with the EUPHORE studies, the theoretical

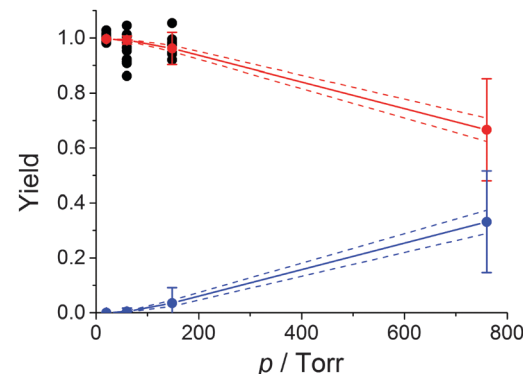


**Fig. 4** Experimental HO<sub>2</sub> yield (black circles) and calculated HO<sub>2</sub> and HOCH<sub>2</sub>CH(O<sub>2</sub>)NH<sub>2</sub> yields (red circles and line and blue circles and line, respectively) using MESMER for HOCH<sub>2</sub>CHNH<sub>2</sub> + O<sub>2</sub> reaction at 298 K and various pressures of nitrogen bath gas. The error bars were calculated by varying the energy barrier for the formation of HO<sub>2</sub> by  $\pm 4$  kJ mol<sup>-1</sup>. The dash lines show the propagation of the statistical errors obtained by fitting the experimental points.

calculations carried out by da Silva found that, at atmospheric pressure, the reaction largely bypasses the collisional stabilisation (R7) to proceed through reaction (R5).<sup>40</sup>

In order to determine the branching ratios  $r_5$  and  $r_7$  at atmospheric pressure we performed master equation calculations using the MESMER package, details of which can be found elsewhere.<sup>32,33</sup> MESMER solves the master equation and the subsequent eigenvalue–eigenvector analysis outputs the time profiles of species concentrations together with the phenomenological rate constants of the system.

A negative pressure dependence of the HO<sub>2</sub> yield and a corresponding positive dependence of the RO<sub>2</sub> yield ( $\Gamma_{\text{RO}_2}$ ) were obtained (Fig. 4), in agreement with previous studies of O<sub>2</sub> reactions with RCHNHR radicals.<sup>32</sup> At atmospheric pressure our result,  $\Gamma_{\text{RO}_2} = 0.33 \pm 0.18$ , is in agreement with the calculation of da Silva using the same value for  $\Delta E_{\text{down}}$  as our work, 270 cm<sup>-1</sup>,  $\Gamma_{\text{RO}_2} = 0.23$ , and disagrees with EUPHORE result,  $\Gamma_{\text{RO}_2} = 1$ .<sup>23,25</sup>

## 4. Atmospheric modelling

### 4.1. Model description

Simulations were performed for the Mongstad PCCC plant emissions using two chemical box models. The first model contained typical gas-phase concentrations of volatile organic compounds (VOCs) observed at a European coastal background site – Mace Head, Ireland.<sup>41</sup> The background concentrations of NO, NO<sub>2</sub> and O<sub>3</sub> were constrained to the hourly averaged diurnal cycles measured for the north-westerly wind sector at the Weybourne Atmospheric Observatory located on the Norfolk coast of England in September 2002 (Fig. S7–S9, ESI<sup>†</sup>).<sup>42,43</sup> The Weybourne data are representative for summer conditions and have been chosen as their daily averages: [O<sub>3</sub>] = 39 ppbv, [NO] = 0.3 ppbv and [NO<sub>2</sub>] = 3 ppbv best describe the moderately polluted background conditions at Mongstad.<sup>34</sup> The background model was based on detailed chemistry from the Master Chemical



Mechanism (MCM v3.2), with the extracted model chemical mechanism containing 2255 species participating in 6920 gas-phase reactions.<sup>44,45</sup> The model was run for four days re-initialising the background concentrations after each day, in order to generate model intermediate species in steady state. Fig. S10 (ESI†) shows the diurnal cycle of OH radical as an example. The concentrations at the end of four days were input in a second box model (the plume model), which contained both the background reactions and the OH initiated oxidation of the emitted MEA (*vide infra*), which was run for a further day. The time steps in the numerical simulations were 15 seconds in the clear day scenario and 1 second in the cloudy day scenario (*vide infra*). During these simulations the concentrations of NO<sub>2</sub> and O<sub>3</sub> were constrained to the one minute averages measured at Weybourne in September 2002 (ESI†).<sup>42,43</sup> As the PCCC emits NO (133 tonnes per annum),<sup>34</sup> the [NO] in the plume initially exceeds [NO] outside the plume and hence it is diluted to ambient values by the plume dispersion (*vide infra*).

The amine chemistry scheme used in the plume model contained 20 species involved in 24 gas-phase reactions, reversible partitioning of MEA and the nitrosamine and nitramine products between the gas-phase and aqueous phase particles, and reactions of MEA, R<sub>2</sub>N-NO and R<sub>2</sub>N-NO<sub>2</sub> with OH in the liquid phase (ESI†). Heterogeneous uptake was represented by a parameterization of a first-order loss process to the aerosol surface:<sup>46</sup>

$$k_f' = \left( \frac{r}{D_i^g} + \frac{4}{\gamma_i \bar{c}_i^g} \right)^{-1} A \quad (E4)$$

where  $k_f'$  is the first-order rate coefficient for heterogeneous loss,  $r$  is the aerosol particle effective radius,  $D_i^g$  is the gas-phase diffusion coefficient of the species  $i$ ,  $\gamma_i$  is the uptake coefficient for the gas  $i$ ,  $\bar{c}_i^g$  is the mean molecular speed of  $i$  and  $A$  is the aerosol surface area per unit volume. More details on the parameters used in the calculation of  $k_f'$  are given in ESI†. The first-order rate coefficient describing the transfer from aerosol to gas-phase,  $k_b'$ , was calculated using the Henry's law coefficient,  $H_i$ :<sup>34</sup>

$$\frac{k_f'}{k_b'} = RTH_i \quad (E5)$$

Here  $R$  is the gas constant,  $T$  is the temperature in Kelvin and  $H_i = \frac{[i]_{aq}}{p_i}$ , where  $[i]_{aq}$  is the molar concentration of compound  $i$  in the aqueous particles and  $p_i$  is the partial pressure of gas  $i$  in the plume emitted by the PCCC plant.

Two scenarios were studied: a clear day where  $r = 0.5 \mu\text{m}$  and atmospheric liquid water content,  $g_w = 10^{-4} \text{ g m}^{-3}$ ,<sup>47,48</sup> and a cloudy day where  $r = 10 \mu\text{m}$  and  $g_w = 0.5 \text{ g m}^{-3}$ .<sup>19,47</sup> In the cloudy day scenario an attenuation of the actinic flux by a factor of 0.5 relative to the actinic flux under clear sky conditions was applied.<sup>49</sup> Under the clear sky conditions emissions were set at 10:00, 14:00 and 24:00, while under the cloudy sky conditions the emissions were set at 10:00.

Emissions were set to  $1.27 \text{ g s}^{-1}$  of MEA (40 tonnes per year) and  $4.22 \text{ g s}^{-1}$  of NO<sup>34</sup> in mid-July and  $T = 288.15 \text{ K}$ . Species concentrations within the PCCC plume were modelled within a

well-mixed box transported in downwind direction. Numerical simulations were started at 10 min after emission, when the plume was considered to have filled the boundary layer (set to 1000 m depth) by vertical mixing. Therefore, the box had a fixed height of 1000 m. The width of the plume,  $y(t)$ , has been expanding *via* horizontal (cross-flow) mixing with the ambient air starting from  $y(0) = 3816 \text{ m}$  at day time and from  $y(0) = 1658 \text{ m}$  at night (ESI†).<sup>50,51</sup>

$$y(t) = [y(0)^2 + 8K_y t]^{1/2} \quad (E6)$$

Here  $K_y$  is the horizontal diffusion coefficient,  $3034 \text{ m}^2 \text{ s}^{-1}$  for day time emissions and  $573 \text{ m}^2 \text{ s}^{-1}$  for the midnight emission (ESI†).

The emitted amine, NO and the targeted products nitrosamine (R<sub>2</sub>N-NO) and nitramine (R<sub>2</sub>N-NO<sub>2</sub>), were diluted with ambient air according to a Gaussian equation:

$$\frac{d[i]_g}{dt} = -\frac{4K_y}{[y(0)^2 + 8K_y t]} ([i]_g - [i]_g^b) \quad (E7)$$

where  $[i]_g$  is the gas-phase concentration of compound  $i$  within the plume and  $[i]_g^b$  is the concentration of  $i$  outside the plume. In order to describe the time evolution of NO, a separate model was used to simulate the dispersion of the emitted NO to ambient values (eqn (E7)). Ambient NO was constrained to the one minute averaged diurnal cycle of NO measured at Weybourne.<sup>42</sup> During each box model simulation incorporating the amine emission, NO was constrained to follow the profile generated by the dispersion model (see Fig. S12 as an example, ESI†), while NO<sub>2</sub> and O<sub>3</sub> were constrained to Weybourne data (*vide supra*).

#### 4.2. Results of the simulations

**4.2.1. Day time emissions in the clear day and the cloudy day.** The MEA losses under clear sky conditions are: 48% reaction with OH and 52% dispersion for emission at 10:00 and 51% reaction with OH and 49% dispersion for emission at 14:00, with heterogeneous uptake negligible in both cases. In the cloudy day simulation, emission at 10:00, MEA losses are: 93% uptake, 4% gas-phase reaction and 3% dispersion. Therefore, under cloudy conditions, only a relatively small fraction of MEA is available for reaction with OH in gas-phase. Fig. 5 and 6 show the rates of the MEA losses emitted at 10:00 under clear and cloudy sky conditions, respectively. The dominant clear sky losses, dispersion and reaction with OH, become minor in the cloudy day scenario, where the initial rate of uptake is two orders of magnitude faster than the rates of dispersion and reaction. MEA is almost completely removed in the first 2–3 hours after emission in the clear day and in about one minute in the cloudy day.

Fig. 7 and 8 show the concentrations of nitramine and nitrosamine in the PCCC plume *vs.* time and downwind distance from the emission point in the cloud free and cloudy sky scenarios, respectively. The time was converted into distance by using a wind speed of  $3 \text{ m s}^{-1}$ . Fig. 7a shows the profile of nitramine concentration for emissions at 10:00 and 14:00. Emissions at 10:00 and 14:00 amplifies gas phase chemistry as at 10:00 NO



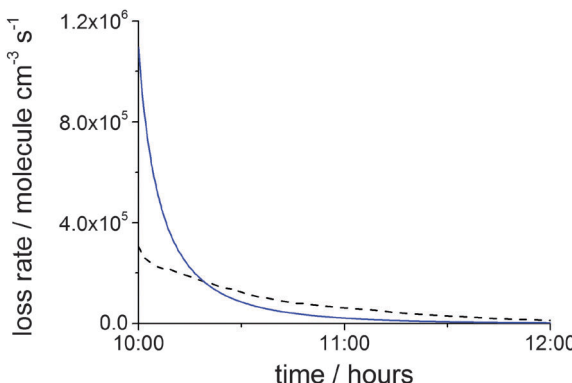


Fig. 5 Loss rates of MEA vs. day time following the emission from PCCC plant at 10:00 under clear sky conditions: dispersion rate (blue solid line) and rate of the OH + MEA reaction (black dash line). With the exception of the first minute, when the uptake rate of MEA is  $\sim 5 \times 10^5$  molecule  $\text{cm}^{-3} \text{s}^{-1}$ , Henry's law is fulfilled for almost all of the simulation time and hence almost no uptake of MEA onto aerosols occurs.

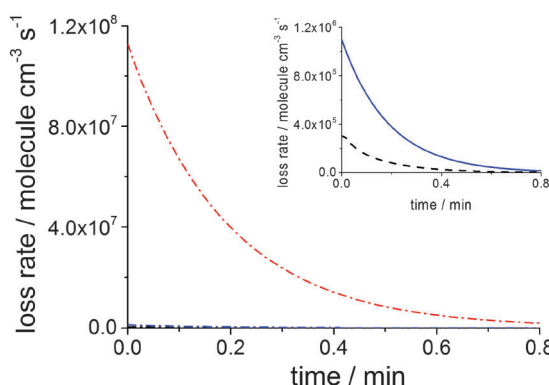


Fig. 6 Time evolution of the loss rates of MEA emitted by PCCC plant at 10:00 in the cloudy day scenario: uptake rate (red dash dot line), dispersion rate (blue solid line) and rate of the OH + MEA reaction (black dash line). The inset shows the dispersion rate and the reaction rate magnified. Time zero in numerical simulations corresponds to 10 min after emission.

and  $\text{NO}_2$  reach their maximum, while at 14:00  $\text{O}_3$  peaks, maximising OH concentration (ESI†). The maximum of  $[\text{R}_2\text{N}-\text{NO}_2]$  is  $\sim 30\%$  higher for the 10:00 emission than in the 14:00 scenario and is three times above the current safe guideline level of  $0.3 \text{ ng m}^{-3}$  (annual average), as established by the Norwegian Institute for Public Health (NIPH).<sup>21</sup> Owing to a lack of toxicity data on nitramines, the NIPH decided to use the cancer risk estimated for *N*-nitrosodimethylamine (DMA-NO) for the sum of the concentrations of nitramines and nitrosamines in air. The restriction of the air level of total nitramines and nitramines to  $0.3 \text{ ng m}^{-3}$  may be regarded as a conservative limit as DMA-NO was found to have  $\sim 6$  times higher cancer potency than *N*-nitrodimethylamine, DMA- $\text{NO}_2$ .<sup>21</sup> However, recent studies reported that DMA- $\text{NO}_2$  is less toxic than 2-nitroaminoethanol and emphasized the need for additional investigations of the cancer potency of nitramines.<sup>52</sup>

For both 10:00 and 14:00 cases the concentration of  $\text{R}_2\text{N}-\text{NO}_2$  reaches its maximum after *ca.* 11 km ( $\sim 1$  hour), where  $\text{R}_2\text{N}-\text{NO}_2$  formation becomes less significant than  $\text{R}_2\text{N}-\text{NO}$ .

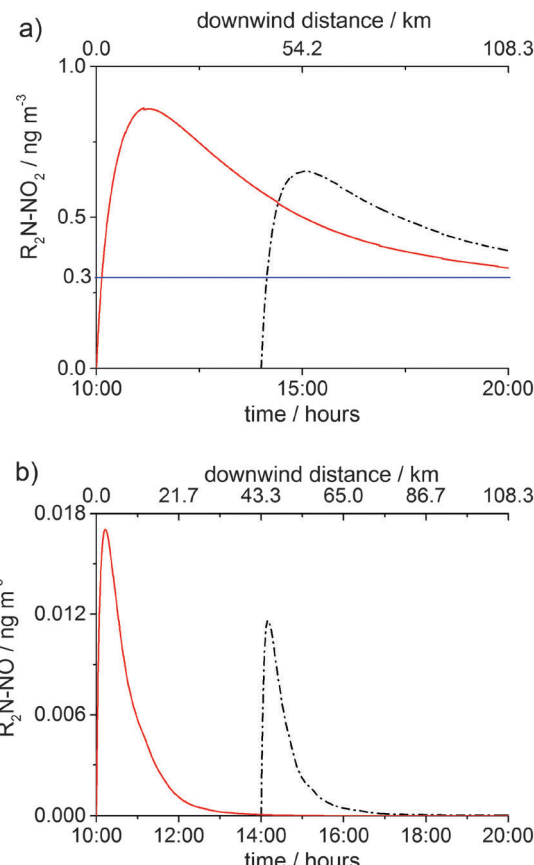


Fig. 7 Gas-phase concentrations of (a)  $\text{R}_2\text{N}-\text{NO}_2$  and (b)  $\text{R}_2\text{N}-\text{NO}$  in the PCCC plume as a function of time (bottom axis) in the clear day scenario. Emission time: 10:00 (red solid line) and 14:00 (black dash dot line). The top axis shows the downwind distance from the source for the emission at 10:00. The horizontal blue line in (a) shows the safety limit of  $0.3 \text{ ng m}^{-3}$  for  $[\text{R}_2\text{N}-\text{NO}_2] + [\text{R}_2\text{N}-\text{NO}]$  established by the NIPH.<sup>21</sup>

loss (OH reaction and dispersion).  $[\text{R}_2\text{N}-\text{NO}_2]$  goes below the health limit after  $\sim 130$  km downwind of the emission. The concentration of nitrosamine peaks early (after  $\sim 12$  min or 2 km from source) at a value about 20 times lower than the safety limit ( $0.3 \text{ ng m}^{-3}$ ), after which photolytic degradation and dispersion start to dominate.

Assuming that nitrosamine isomerises as soon as it is formed leading to an imine,<sup>23,25,30</sup> for emission at 10:00 under clear sky conditions, the obtained concentration of  $\text{R}_2\text{N}-\text{NO}_2$  is practically the same as  $[\text{R}_2\text{N}-\text{NO}_2]$  obtained considering that nitrosamine does not isomerise but photolyses to generate back  $\text{R}_2\text{N}$  radical. Note that, assuming nitrosamine formation, the rate of nitramine formation is 10 times higher than the rate of nitrosamine formation.

Fig. 8 shows that, under cloudy conditions, the maximum value of  $[\text{R}_2\text{N}-\text{NO}_2] + [\text{R}_2\text{N}-\text{NO}]$  is  $\sim 75$  times lower than the safety level. After a brief increase (over the first 12 s of the numerical simulation), both  $\text{R}_2\text{N}-\text{NO}_2$  and  $\text{R}_2\text{N}-\text{NO}$  are almost completely removed from the gas-phase within 90 s by heterogeneous uptake.

**4.2.2. Midnight emission under clear sky conditions.** Numerical simulations performed using the background model

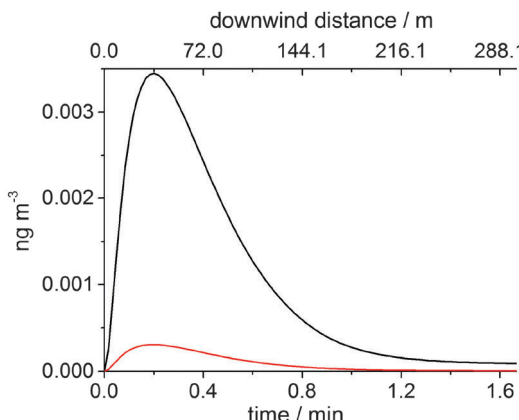


**Fig. 8** Air concentrations of  $\text{R}_2\text{N-NO}_2$  (black line) and  $\text{R}_2\text{N-NO}$  (red line) as a function of time (bottom axis) and downwind distance (top axis) following the emission from PCCC plant at 10:00 in the cloudy day scenario. Time zero in numerical simulations corresponds to 10 min after emission, i.e. 1.8 km.

shows that the concentration of  $\text{NO}_3$  radicals (the dominate night time oxidant)<sup>53</sup> peaks at  $\sim 10^8$  molecule  $\text{cm}^{-3}$  at midnight. Similarly to OH,  $\text{NO}_3$  abstracts from both C-H and N-H sites of amines. Abstraction at the N-H site generates a nitrogen-centred radical which produces nitrosamine and nitramine by reacting with NO (reaction (R2)) and  $\text{NO}_2$  (reaction (R3)).

The rate coefficient of the reaction of MEA with  $\text{NO}_3$ ,  $k_{\text{MEA+NO}_3}$ , has not been determined experimentally. Karl *et al.* calculated  $k_{\text{MEA+NO}_3} = 1.5 \times 10^{-13} \text{ cm}^3 \text{ molecule}^{-1} \text{ s}^{-1}$  using a structure-property relationship,<sup>23</sup> in good agreement with the SAR estimate  $k_{\text{MEA+NO}_3} = 1.4 \times 10^{-13} \text{ cm}^3 \text{ molecule}^{-1} \text{ s}^{-1}$  found by Carter.<sup>54</sup> However, assuming that the linear correlation between the reactions of OH and  $\text{NO}_3$  with the same substrate<sup>19,53</sup> is followed by amines, a value of  $1 \times 10^{-12} \text{ cm}^3 \text{ molecule}^{-1} \text{ s}^{-1}$  is obtained for  $k_{\text{MEA+NO}_3}$ . As shown below, using the higher estimates for the rate coefficient of  $\text{NO}_3$  with MEA leads to significant nitramine and nitrosamine formation. In addition, there are no data available for branching in the MEA +  $\text{NO}_3$  reaction. Here we consider the worst case scenario where 100% of the MEA +  $\text{NO}_3$  reaction proceeds to nitrogen-centred radical.

Fig. 9a and b show the time and the downwind distance dependences of  $[\text{R}_2\text{N-NO}_2]$  and  $[\text{R}_2\text{N-NO}]$ , respectively in three cases: the MEA +  $\text{NO}_3$  reaction is negligible and hence not considered in the model (the base case),  $k_{\text{MEA+NO}_3} = 1.5 \times 10^{-13} \text{ cm}^3 \text{ molecule}^{-1} \text{ s}^{-1}$  and  $k_{\text{MEA+NO}_3} = 1 \times 10^{-12} \text{ cm}^3 \text{ molecule}^{-1} \text{ s}^{-1}$ . By using  $k_{\text{MEA+NO}_3} = 1.5 \times 10^{-13} \text{ cm}^3 \text{ molecule}^{-1} \text{ s}^{-1}$  an 8% increase over the base case in the total nitramine formed in the first 24 hours after emission is produced, while the value of  $1 \times 10^{-12} \text{ cm}^3 \text{ molecule}^{-1} \text{ s}^{-1}$  produces a 50% increase in the total nitramine formed in the first 24 hours. The change in the total nitrosamine generated over one day is more significant due to the lack of photolytic destruction at night: a 20% increase using  $1.5 \times 10^{-13} \text{ cm}^3 \text{ molecule}^{-1} \text{ s}^{-1}$  and a 100% increase using  $1 \times 10^{-12} \text{ cm}^3 \text{ molecule}^{-1} \text{ s}^{-1}$ . In all three midnight scenarios the total amount of carcinogenic compounds formed over 24 hours is significant, several times larger than the one produced by the day time emissions (*vide supra*).

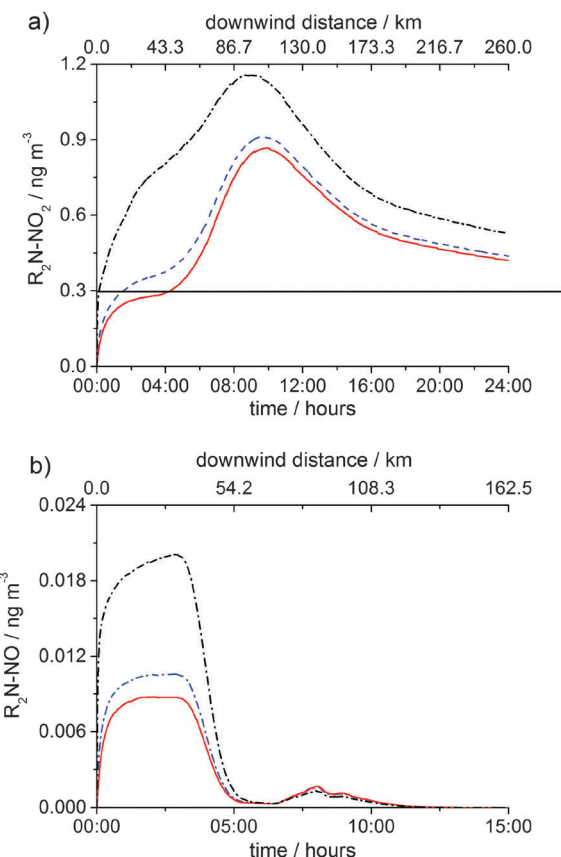


**Fig. 9** Gas-phase concentrations of (a)  $\text{R}_2\text{N-NO}_2$  and (b)  $\text{R}_2\text{N-NO}$  in the PCCC plume as a function of time (bottom axis) and downwind distance (top axis) from emission point under clear sky conditions and midnight emission scenario: no MEA +  $\text{NO}_3$  reaction (red solid line),  $k_{\text{MEA+NO}_3} = 1.5 \times 10^{-13} \text{ cm}^3 \text{ molecule}^{-1} \text{ s}^{-1}$  (blue dash line) and  $k_{\text{MEA+NO}_3} = 1 \times 10^{-12} \text{ cm}^3 \text{ molecule}^{-1} \text{ s}^{-1}$  (black dash dot line). The horizontal black line in (a) shows the safety limit of  $0.3 \text{ ng m}^{-3}$  for  $[\text{R}_2\text{N-NO}_2] + [\text{R}_2\text{N-NO}]$  established by the NIPH.<sup>21</sup>

In all three midnight scenarios, dispersion is the main loss of MEA within the first five hours. As the dispersion rate decreases fast in time (eqn (E7)) and in the morning OH concentration starts to increase, between 05:00–10:00 the rate of the MEA + OH reaction increases, dominating over the dispersion rate (Fig. S13, ESI†) and leading to more nitramine formation. After reaching a maximum of about 3–4 times above the safety level at  $\sim 10:00$ , nitramine is consumed by reaction with OH (Fig. 9a). Nitrosamine formed during the night is 15–30 times lower than the tolerance limit and photolyses rapidly upon sunrise (Fig. 9b). A small increase in  $\text{R}_2\text{N-NO}$  occurs between 06:30–08:00 due to the increase in both OH and NO levels in the morning.

**4.2.3. Comparison with the previous atmospheric modelling studies.** Previous studies of the formation of nitrosamines and nitramines by the atmospheric oxidation of carbon capture amines have addressed the MEA emissions from the Mongstad PCCC pilot plant using chemical transport models,<sup>24,34,55</sup> incorporating much more simplified atmospheric chemistry schemes than used in this study, as well as dispersion and wet deposition. In addition, Karl *et al.* included dry deposition. The present study uses the MEA and



NO emissions reported by Karl *et al.*<sup>34</sup> In the study of Karl *et al.* the yearly average sum of the concentrations of  $R_2N\text{-NO}$  and  $R_2N\text{-NO}_2$  at ground level air is 1 to 3 orders of magnitude lower than the safety limit of  $0.3 \text{ ng m}^{-3}$ .<sup>21,34</sup> These results are explained by a relatively small contribution of the reaction with OH to the total yearly MEA removal. In the baseline case used by Karl *et al.*, the yearly average losses of MEA in a  $200 \text{ km} \times 200 \text{ km}$  area around the PCCC were: ~50% transport by diffusion and advection, 29% dry deposition, 17% wet deposition and 5% reaction with OH.

The previous investigations used a branching ratio for OH abstraction at  $\text{NH}_2$  group of 0.08<sup>34,55</sup> while here we considered that the abstraction at N-H site to be ~5 times greater ( $r_{1b} = 0.38$ ).<sup>31</sup> Karl *et al.* identified that the branching ratios in the initial amine + OH reaction is one of the main uncertainties affecting their results.<sup>34</sup> In line with these authors we have found that the sum of air concentrations of  $R_2N\text{-NO}$  and  $R_2N\text{-NO}_2$  increases linearly with the branching ratio for the OH abstraction at the N-H site. Koeijer *et al.*<sup>55</sup> found that  $[\text{R}_2\text{N-NO}_2] + [\text{R}_2\text{N-NO}]$  is 30–180 times lower than the defined safety level for emissions of MEA 10–60 times lower than in the present work and Karl *et al.*<sup>34</sup>

Our work treats the atmospheric chemistry in detail, while using a simple representation of the dispersion of amines and their toxic degradation products. The results show that, under cloud free conditions, for both day and night PCCC emissions, nitramine can reach levels significantly above the generally adopted tolerance limit of  $0.3 \text{ ng m}^{-3}$ . The peak concentration for our scenario (horizontal wind speed of  $3 \text{ m s}^{-1}$ ) is at distance of *ca.* 10 km (~1 hour) from the source for the daytime emissions and *ca.* 100 km (~10 hours) from the emission point for the midnight scenario. For both day and night emissions the safety limit is still not met after 100 km away from the point of maximum health risk. The results obtained for the midnight scenario are more uncertain as  $k_{\text{MEA+NO}_3}$  and the H atom abstraction branching ratios in the MEA +  $\text{NO}_3$  reaction are not well known. Results of numerical simulations using estimates of  $k_{\text{MEA+NO}_3}$  are very sensitive to the value of this parameter. An order of magnitude increase of  $k_{\text{MEA+NO}_3}$  generates an important increase in the total amount of gas-phase toxic products formed over 24 hours after emission, by 50% for nitramine and by 100% for nitrosamine. It is therefore important that more research is carried out in order to constrain the rate constants and H-abstraction branching ratios in the reaction of  $\text{NO}_3$  with ethanol amines.

## 5. Conclusions

The rate coefficients for the OH radical reactions with *N*-methylethanolamine (MMEA) and *N,N*-dimethylethanolamine (DMEA) have been determined as a function of temperature using the laser flash photolysis – laser induced fluorescence technique. The result for the OH + DMEA reaction is similar to previous results reported for a series of OH + amine reactions.<sup>13–15</sup> This is the first kinetic study of the OH + MMEA reaction and shows that the room temperature rate coefficient  $k_{\text{OH+MMEA}}$  and its temperature dependence are close to the results obtained for the

OH + MEA reaction.<sup>16</sup> The rate coefficients for both MMEA and DMEA at 298 K are in good agreement with the calculations using the structure–activity relationships (SARs).<sup>19,27,28</sup>

Similarly to the OH + trimethylamine (TMA)/ $\text{O}_2$  reaction, the OH + DMEA/ $\text{O}_2$  reaction has been found to recycle OH. The result suggests that OH recycling through a chemical activated peroxy radical is a common signature for tertiary amines.

The dominant abstraction site in the OH reaction with monoethanolamine (MEA), MMEA and DMEA has been found to be the methylene group next to the amine group. The branching ratio for abstraction at the  $\alpha\text{-C-H}$  site of MEA is in between the value obtained by the EUPHORE atmospheric chamber study of Karl *et al.*<sup>23</sup> and the value calculated using SARs (ESI<sup>†</sup>). Abstraction at the  $\alpha\text{-C-H}$  site generates a  $\text{HOCH}_2\text{CHNR}$  radical, which reacts further with  $\text{O}_2$ . Calculations using MESMER<sup>56</sup> shows that at atmospheric pressure the  $\text{HOCH}_2\text{CHNR} + \text{O}_2$  reaction occurs predominantly through the abstraction route, producing  $\text{HO}_2$  and 2-iminoethanol. The result is in agreement with previous findings for  $\text{O}_2$  reactions with  $\text{RCHNHR}$  ( $\text{R} = \text{CH}_3$  or H) radicals.<sup>19,32,57</sup>

The production of carcinogenic nitramines and nitrosamines depends on the branching ratio for abstraction at the N-H site,  $r_{\text{N-H}}$ . As  $r_{\text{N-H}}$  is higher for MMEA than for the standard post-combustion carbon capture (PCCC) solvent MEA, MMEA has a higher potential to form toxic compounds by atmospheric oxidation than MEA.

The health risks due to the formation of carcinogenic compounds following a typical MEA emission into the troposphere are assessed using a modified box model focusing on the detailed chemistry. Model plume emissions are based on the Mongstad PCCC pilot plant, located on the west coast of Norway. The results show that on clear, cloud free days concentrations of carcinogenic nitramine formed by the atmospheric photo-oxidation of the benchmark PCCC solvent MEA, exceed the recommended annual average value of  $0.3 \text{ ng m}^{-3}$ . The studies also show that heterogeneous uptake significantly reduces atmospheric concentrations and so the annual average concentration will be very dependent on local meteorology.

## Acknowledgements

This work was supported by grants from NERC (NE/1013474/1) and EPSRC (EP/J010871/1). The authors thank Prof. Chris Rayner for useful discussions on synthesis issues, Prof. Nielsen, University of Oslo, for on-going discussions and providing unpublished results from the Atmospheric Degradation of Amines (ADA) project supported by Masdar, Statoil, Vattenfall, Shell and the CLIMIT program under contracts 193438, 201604 and 208122, Dr Jenny Young for useful discussions regarding atmospheric modelling, Lucy Thonger for help with some of the experiments and Dr Zoe Fleming, NCAS, University of Leicester for supplying the Weybourne data.

## References

- 1 M. E. Boot-Handford, J. C. Abanades, E. J. Anthony, M. J. Blunt, S. Brandani, N. Mac Dowell, J. R. Fernandez, M. C. Ferrari,

R. Gross, J. P. Hallett, R. S. Haszeldine, P. Heptonstall, A. Lyngfelt, Z. Makuch, E. Mangano, R. T. J. Porter, M. Pourkashanian, G. T. Rochelle, N. Shah, J. G. Yao and P. S. Fennell, *Energy Environ. Sci.*, 2014, **7**, 130–189.

2 L. Zhu, G. W. Schade and C. J. Nielsen, *Environ. Sci. Technol.*, 2013, **47**, 14306–14314.

3 E. F. da Silva and A. M. Booth, *Environ. Sci. Technol.*, 2013, **47**, 659–660.

4 C. H. Yu, C. H. Huang and C. S. Tan, *Aerosol Air Qual. Res.*, 2012, **12**, 745–769.

5 Y. Zhang, J. Xu, Y. Zhang, J. Zhang, Q. Li, H. Liu and M. Shang, *Int. J. Greenhouse Gas Control*, 2014, **20**, 37–42.

6 E. S. Rubin, H. Mantripragada, A. Marks, P. Versteeg and J. Kitchin, *Prog. Energy Combust. Sci.*, 2012, **38**, 630–671.

7 G. T. Rochelle, *Science*, 2009, **325**, 1652–1654.

8 C. Gouedard, D. Picq, F. Launay and P. L. Carrette, *Int. J. Greenhouse Gas Control*, 2012, **10**, 244–270.

9 I. Eide-Haugmo, H. Lepaumier, A. Einbu, K. Vernstad, E. F. da Silva and H. F. Svendsen, *Energy Procedia*, 2011, **4**, 1631–1636.

10 P. Bruder, K. G. Lauritsen, T. Mej dell and H. F. Svendsen, *Chem. Eng. Sci.*, 2012, **75**, 28–37.

11 A. Chakma and A. Meisen, *J. Chromatogr.*, 1988, **457**, 287–297.

12 K. Veltman, B. Singh and E. G. Hertwich, *Environ. Sci. Technol.*, 2010, **44**, 1496–1502.

13 L. Onel, L. Thonger, M. A. Blitz, P. W. Seakins, A. J. C. Bunkan, M. Solimannejad and C. J. Nielsen, *J. Phys. Chem. A*, 2013, **117**, 10736–10745.

14 S. A. Carl and J. N. Crowley, *J. Phys. Chem. A*, 1998, **102**, 8131–8141.

15 R. Atkinson, R. A. Perry and J. N. Pitts, Jr., *J. Chem. Phys.*, 1978, **68**, 1850–1853.

16 L. Onel, M. A. Blitz and P. W. Seakins, *J. Phys. Chem. Lett.*, 2012, **3**, 853–856.

17 N. Borduas, J. P. D. Abbatt and J. G. Murphy, *Environ. Sci. Technol.*, 2013, **47**, 6377–6383.

18 L. Onel, M. Dryden, M. A. Blitz and P. W. Seakins, *Environ. Sci. Technol. Lett.*, 2014, **1**, 367–371.

19 C. J. Nielsen, H. Herrmann and C. Weller, *Chem. Soc. Rev.*, 2012, **41**, 6684–6704.

20 J. M. Nicovich, S. Mazumder, P. L. Laine, P. H. Wine, Y. Tang, A. J. C. Bunkan and C. J. Nielsen, *Phys. Chem. Chem. Phys.*, 2015, **17**, 911–917.

21 M. Låg, B. Lindeman, C. Instanes, G. Brumborg and P. Schwarze, *Health Effects of Amines and Derivatives Associated with CO<sub>2</sub> Capture*, The Norwegian Institute of Public Health, 2011.

22 X. L. Ge, A. S. Wexler and S. L. Clegg, *Atmos. Environ.*, 2011, **45**, 524–546.

23 M. Karl, C. Dye, N. Schmidbauer, A. Wisthaler, T. Mikoviny, B. D'Anna, M. Muller, E. Borras, E. Clemente, A. Munoz, R. Porras, M. Rodenas, M. Vazquez and T. Brauers, *Atmos. Chem. Phys.*, 2012, **12**, 1881–1901.

24 M. Karl, R. F. Wright, T. F. Berglen and B. Denby, *Int. J. Greenhouse Gas Control*, 2011, **5**, 439–447.

25 C. J. Nielsen, B. D'Anna, C. Dye, M. Graus, M. Karl, S. King, M. M. Maguto, M. Mueller, N. Schmidbauer, Y. Stenstrom, A. Wisthaler and S. Pedersen, *Energy Procedia*, 2011, **4**, 2245–2252.

26 H.-B. Xie, C. Li, N. He, C. Wang, S. Zhang and J. Chen, *Environ. Sci. Technol.*, 2014, **48**, 1700–1706.

27 P. J. Ziemann and R. Atkinson, *Chem. Soc. Rev.*, 2012, **41**, 6582–6605.

28 E. S. C. Kwok and R. Atkinson, *Atmos. Environ.*, 1995, **29**, 1685–1695.

29 Y. Z. Tang and C. J. Nielsen, *Atmos. Environ.*, 2012, **55**, 185–189.

30 Y. Tang, M. Hanrath and C. J. Nielsen, *Phys. Chem. Chem. Phys.*, 2012, **14**, 16365–16370.

31 G. da Silva, *Environ. Sci. Technol.*, 2013, **47**, 7766–7772.

32 L. Onel, M. Blitz, M. Dryden, L. Thonger and P. Seakins, *Environ. Sci. Technol.*, 2014, **48**, 9935–9942.

33 D. R. Glowacki, C.-H. Liang, C. Morley, M. J. Pilling and S. H. Robertson, *J. Phys. Chem. A*, 2012, **116**, 9545–9560.

34 M. Karl, N. Castell, D. Simpson, S. Solberg, J. Starrfelt, T. Svendby, S. E. Walker and R. F. Wright, *Atmos. Chem. Phys.*, 2014, **14**, 8533–8557.

35 S. A. Carr, M. T. Baeza-Romero, M. A. Blitz, B. J. S. Price and P. W. Seakins, *Int. J. Chem. Kinet.*, 2008, **40**, 504–514.

36 S. Kapteina, K. Slowik, S. P. Verevkin and A. Heintz, *J. Chem. Eng. Data*, 2005, **50**, 398–402.

37 G. W. Harris and J. N. Pitts, *Environ. Sci. Technol.*, 1983, **17**, 50–51.

38 L. G. Anderson and R. D. Stephens, *Int. J. Chem. Kinet.*, 1988, **20**, 103–110.

39 S. A. Carr, D. R. Glowacki, C.-H. Liang, M. T. Baeza-Romero, M. A. Blitz, M. J. Pilling and P. W. Seakins, *J. Phys. Chem. A*, 2011, **115**, 1069–1085.

40 G. da Silva, *J. Phys. Chem. A*, 2012, **116**, 10980–10986.

41 A. C. Lewis, K. D. Bartle, D. E. Heard, J. B. McQuaid, M. J. Pilling and P. W. Seakins, *J. Chem. Soc., Faraday Trans.*, 1997, **93**, 2921–2927.

42 Z. L. Fleming, *Personal communication of diurnal cycles of O<sub>3</sub>, NO and NO<sub>2</sub> measured at Weybourne between 17 and 29 September 2002*.

43 Z. L. Fleming, P. S. Monks, A. R. Rickard, B. J. Bandy, N. Brough, T. J. Green, C. E. Reeves and S. A. Penkett, *Atmos. Chem. Phys.*, 2006, **6**, 5415–5433.

44 <http://mcm.leeds.ac.uk/MCM>.

45 S. M. Saunders, M. E. Jenkin, R. G. Derwent and M. J. Pilling, *Atmos. Chem. Phys.*, 2003, **3**, 161–180.

46 S. E. Schwartz, in *Chemistry of Multiphase Atmospheric Systems*, ed. W. Jaeschke, Springer Berlin Heidelberg, 1986, vol. 6, pp. 415–471.

47 X. L. Ge, A. S. Wexler and S. L. Clegg, *Atmos. Environ.*, 2011, **45**, 561–577.

48 Y. X. Bian, C. S. Zhao, N. Ma, J. Chen and W. Y. Xu, *Atmos. Chem. Phys.*, 2014, **14**, 6417–6426.

49 P. S. Monks, A. R. Rickard, S. L. Hall and N. A. D. Richards, *J. Geophys. Res.: Atmos.*, 2004, **109**, D17206.

50 S. A. Mason, J. Trentmann, T. Winterrath, R. J. Yokelson, T. J. Christian, L. J. Carlson, T. R. Warner, L. C. Wolfe and M. O. Andreae, *J. Atmos. Chem.*, 2006, **55**, 273–297.



51 D. L. Mauzerall, J. A. Logan, D. J. Jacob, B. E. Anderson, D. R. Blake, J. D. Bradshaw, B. Heikes, G. W. Sachse, H. Singh and B. Talbot, *J. Geophys. Res.: Atmos.*, 1998, **103**, 8401–8423.

52 L. M. Fjellsbo, S. Verstraelen, A. Kazimirova, A. R. Van Rompay, Z. Magdolenova and M. Dusinska, *Environ. Res.*, 2014, **134**, 39–45.

53 R. P. Wayne, I. Barnes, P. Biggs, J. P. Burrows, C. E. Canosamas, J. Hjorth, G. Lebras, G. K. Moortgat, D. Perner, G. Poulet, G. Restelli and H. Sidebottom, *Atmos. Environ., Part A*, 1991, **25**, 1–203.

54 W. P. L. Carter, Reactivity Estimates for Selected Consumer Product Compounds Contract No. 06-408, Center for Environmental Research and Technology, College of Engineering, University of California, Riverside, California, USA, 2008.

55 G. de Koeijer, V. R. Talstad, S. Nepstad, D. Tønnessen, O. Falk-Pedersen, Y. Maree and C. Nielsen, *Int. J. Greenhouse Gas Control*, 2013, **18**, 200–207.

56 <http://sourceforge.net/projects/mesmer/>.

57 M. M. Maguta, M. Aursnes, A. J. C. Bunkan, K. Edelen, T. Mikoviny, C. J. Nielsen, Y. Stenstrom, Y. Tang and A. Wisthaler, *J. Phys. Chem. A*, 2014, **118**, 3450–3462.

